Photoluminescent carbon quantum dots from Dichrostachys glomerata pods with antioxidant and Cu 2+ chelating properties

Steve Djiazet, Christophe Desmarets, Hervé Rinnert, Jordane Jasniewski, Ghouti Medjahdi, Lavinia Balan, Raphaël Schneider

Photoluminescent carbon quantum dots from *Dichrostachys glomerata* pods with antioxidant and Cu^{2+} chelating properties

Steve Djiazet,[a] Christophe Desmarets,[b] Hervé Rinnert,[c] Jordane Jasniewski,[d] Ghouti Medjahdi,[c] Lavinia Balan,[e] and Raphaël Schneider*[a]

[a] Dr. S. Djiazet, Dr. R. Schneider

Université de Lorraine, CNRS, LRGP, F-54000 Nancy, France

E-mail : raphael.schneider@univ-lorraine.fr

[b] Dr. C. Desmarets

Sorbonne Université, CNRS, Institut Parisien de Chimie Moléculaire, IPCM, F-75005 Paris, France

[c] Dr. H. Rinnert, G. Medjahdi

Université de Lorraine, CNRS, IJL, F-54000 Nancy, France

[d] Dr. J. Jasniewski

Université de Lorraine, LIBio, F-54000 Nancy, France

[e] Dr. L. Balan

CEMHTI-UPR 3079 CNRS, Site Haute Température, 1D avenue de la Recherche Scientifique, 45071 Orléans, France

Supporting information for this article is given via a link at the end of the document.

Abstract: This work presents the facile and single-step hydrothermal synthesis of carbon quantum dots (CQDs) using the *Dichrostachys glomerata* extract as raw material. CQDs with the highest photoluminescence (PL) were obtained after heating the extract in 4M NaOH at 200°C for 7 h. The obtained CQDs exhibit an average size of ca. 4.7 nm, a green-yellow PL emission independent on the excitation wavelength with contributions located at 478 and 562 nm, a monoexponential decay of their PL lifetime and a PL quantum yield of 18%. These results indicate that the surface functionalization of sp^2 clusters in CQDs is uniform. The antioxidant properties of CQDs were also investigated. CQDs can effectively reduce free radicals like superoxide or oxidants like $KMnO_4$. Moreover, CQDs show a high Cu^{2+} chelating

activity, which is attributed to the abundant carboxylate functions on their surface and may therefore be of high interest in therapeutic applications related to Cu^{2+} ions overload.

Introduction

Dichrostachys glomerata is a shrub present in some African countries (Cameroon, Senegal, Zaire,…), in Asia and in Australia. The fruits of this tree are edible and used as species after drying. The benefits of *D. glomerata* fruits consumption has been demonstrated as they exhibit antioxidant, anti-hypertensive and antibacterial properties as fruits contain bioactive molecules such as phenolic compounds, vitamins and minerals with reactive oxygen species (ROS) scavenging properties. [1-3] Although these antioxidants have shown positive affects in decreasing an oxidative stress, they usually exhibit a modest bioavailability. For example, hydrophilic phenolic compounds including flavones, isoflavones, anthocyanins or chalcones are too hydrophilic to be adsorbed in the gastrointestinal tract while those containing ester functions are decomposed by esterases.[4,5]

Recently, nanoparticles (Ag, CeO_2, MnO_2, ZnO,…) with antioxidant activity have emerged as candidates for decreasing an oxidative stress as they do not only exhibit targeting ability but also because their lifespan in the kidneys is much longer than that of lower molecular weight organic compounds.[6-8] However, their stability in vivo and the release of metal cations pose some safety concerns and could lead to high toxicity. Hence, the development of biocompatible nanoparticles exhibiting antioxidant properties remains a topical issue.

Carbon quantum dots (CQDs) are zero-dimensional nanoparticles with sizes below 10 nm composed of arrangements of $sp^2/sp^3/sp^2$-sp^3 hybridized carbonaceous clusters exhibiting edge effects, defects and their electronic structures are influenced by the quantum confinement effect. The carbon core of CQDs is substituted at the edge by carboxyl, carbonyl, hydroxyl and amino groups which allows these nanoparticles to be easily dispersed in aqueous media and functionalized.[9-13] CQDs have recently gained high interest due to their low cost, high stability and photostability, biocompatibility and tunable photoluminescence (PL) from the UV to the near-infrared and have found many applications in optoelectronic devices or catalysis.[14-17] Their favorable optical properties like high PL quantum yield (QY) and long PL

lifetime have also led to their use in applications such as bio-imaging and sensing.[18,19] CQDs are usually produced via the bottom-up approach by carbonization of precursors (citric acid, urea, amino acids, sugars, …) using solvothermal, hydrothermal, microwave or pyrolysis synthesis processes[9-13] but the CQDs obtained have either no or only weak antioxidant properties. CQDs can also be produced from renewable precursors like biomass-derived materials and some of the properties of the precursor can be transferred to CQDs. [20-22]

In recent years, numerous reports described the synthesis of CQDs exhibiting antioxidant properties including from bioressources. [23-35] This topic is well documented in a recently published review. [36] CQDs produced from vegetable raw materials (tea, flowers, leaves, hydrolysed lignin,…) usually exhibit an excitation wavelength dependent blue to green PL emission as well as radical scavenging properties. Only CQDs produced from chemicals like 1,3,5-trihydroxybenzene have a PL tunable to the yellow region. [33] The CQDs produced have found various applications like bio-imaging,[28] fluorescent sensors for metal cations detection[23,25,34] or antioxidants for food packaging [32,35] or wound healing[33]. Herein, we describe the hydrothermal synthesis of CQDs using the *D. glomerata* extract as raw material. CQDs exhibit a green-yellow PL emission independent on the excitation wavelength with contributions located at 478 and 562 nm and a PL QY of 18%. Due to their high electron transfer ability, CQDs show also antioxidant properties and were demonstrated to effectively reduce $KMnO_4$ and superoxide radicals. The Cu^{2+} chelating properties of CQDs were also evidenced, which could allow CQDs to be valued in therapeutic applications related to Cu^{2+} ions overload.

Figure 1. Schematic illustration of CQDs synthesis from *D. glomerata* pods.

Results and Discussion

CQDs were prepared by hydrothermal treatment of the *D. glomerata* extract in basic medium (Figure 1). In preliminary experiments not described here, the concentration of the extract and of NaOH (1 to 6 M), the temperature (150 to 240°C) and the reaction time (4 to 12 h) were varied. The criterion selected to determine the optimal conditions of CQDs synthesis is the PL intensity. Results obtained show that the highest PL was obtained when CQDs were prepared at 200°C for 7 h using a 4M NaOH solution and these experimental conditions were retained in the rest of the work.

The elemental composition of *D. glomerata* extract and of the derived CQDs was determined by CHONS analyzer (Figure 2a). The starting extract contains 49.77% C, 6.23% H, 39.22% O, 1.24% N, 0.21% S and 2.85% of other elements while the analysis of CQDs shows the presence of 45.95% C, 5.34% H, 35.11% O, 0.37% N, 0.81% S and 6.96% of other elements. These results show that both the extract and CQDs are mainly composed of carbon and oxygen containing functional groups and that CQDs contain very few nitrogen and sulfur functions. Thermogravimetric analysis (TGA) shows that the extract starts to decompose at ca. 200°C and that beyond 600°C, only 2.5% of the initial mass remains, presumably minerals (Figure 2b). As expected, CQDs exhibit a higher stability than the extract. The TGA thermogram of CQDs shows a four-step decomposition pattern. The initial weight loss of ca. 10% can be observed until 200°C and likely corresponds to the removal of water molecules and OH^- anions (see X-ray photoelectron spectroscopy (XPS) paragraph) from the surface of CQDs. The second weight loss of ca. 15% between

200 and 300°C likely corresponds to the decomposition of O containing functional groups (alcohols, carboxylates). A third gradual decline in mass of ca. 15% occurs between 310 and 720°C and could be linked to the reorganization/decomposition of the carbon skeleton. A large mass loss (ca. 40%) is observed from 720 to 800°C and is presumably correlated with the decomposition of the graphitic network. The remaining mass above 1000°C is of 8.74%, which is in relatively good agreement with CHNOS analysis.

Fourier transform infrared (FT-IR) spectroscopy and XPS were used to explore the surface groups and the structure of CQDs. The starting extract shows signals at 3251, 2923, 1700, 1605 and 1039 cm^{-1} corresponding to O-H and N-H, C-H, C=O, C=C and C-O-C bonds, respectively (Figure 2c). These results indicate that the extract contains hydroxyl, amino, carbonyl, alkene and ether functions. All these functions can still be observed in the crude and in the purified CQDs. Noteworthy is also that the signals at 1556 and 1371 cm^{-1} attributed to the carboxylate asymmetric and symmetric stretching modes are the most intense on the purified CQDs, indicating a high density of carboxylate functions at the surface of the dots.

XPS analysis confirms that CQDs are mainly composed of C (78.92%) and O (17.26%) but other elements like Ca, Na, N and Si could also be detected (Figure 3a). The high resolution C 1s XPS spectrum could be deconvoluted into C=C and C-H (285.0 eV), C-O (286.6 eV), C=O and O-C-O (288.10 eV) and O=C-O (289.2 eV) (Figure 3b).[37] The presence of carboxylate, ketone and ether functions agrees well with FT-IR results and is further confirmed by the O 1s XPS spectrum which shows signals at 532.1 eV (O=C-O and C=O), 532.8 eV (C-O) and 533.64 eV (O=C-O) (Figure 3c).[38] The presence of Si (Si-O bond at 531.90 eV) was also confirmed as well as of OH^- anions likely adsorbed at the surface of the dots. We assume that the Si element was one of the unidentified elements present in the *D. glomerata* extract. The high resolution N 1s spectrum indicates the presence of C-N bonds in CQDs (400.22 eV) (Figure 3d).[39] Overall, XPS data agree with FT-IR and confirm that the surface of CQDs is highly functionalized with carboxylate and OH groups, allowing their dispersibility in polar solvents such as water, alcohols (methanol, ethanol), dimethylformamide (DMF) and dimethylsulfoxide (DMSO).

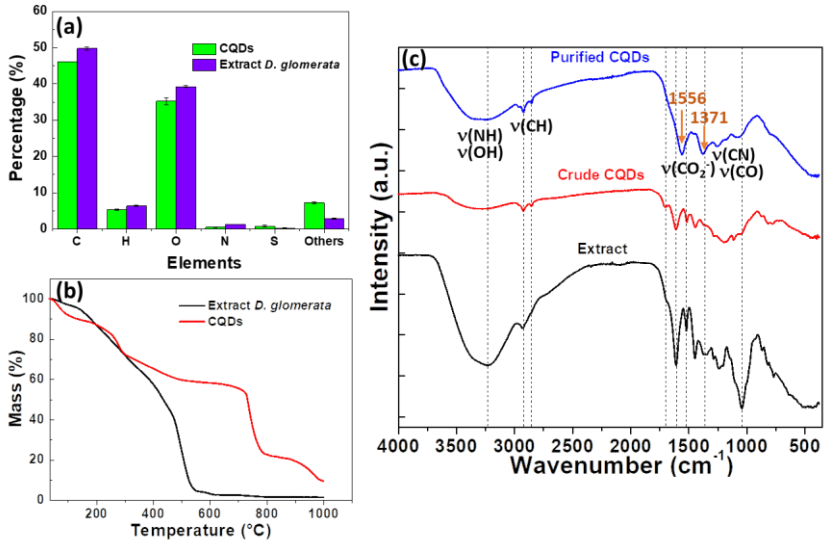

Figure 2. (a) Elemental analyses and (b) TGA traces of the *D. glomerata* extract and of CQDs, (c) FT-IR spectra of the *D. glomerata* extract, of crude and purified CQDs.

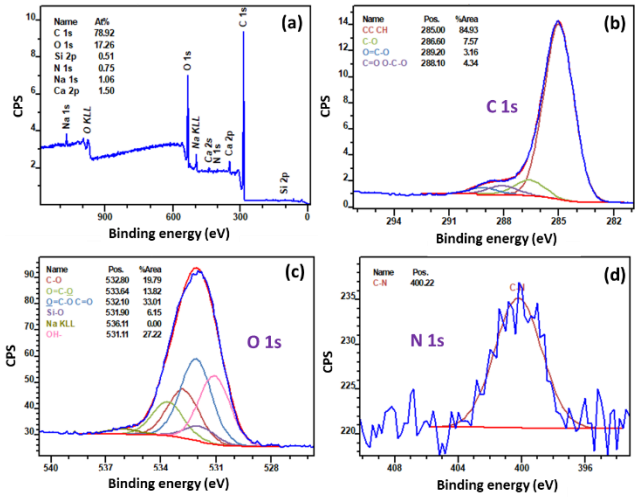

Figure 3. (a) Overview XPS spectrum and high resolution XPS spectra of (b) C 1s, (c) O 1s and (d) N 1s.

The UV-visible absorption spectrum of the extract shows a strong signal at 212 nm that may correspond to the n → π* transition of carboxylic acid functions and to n → σ* transition of amine functions while the signal at 280 nm likely corresponds to UV-visible absorption of polyphenols (Figure 4a).[40] The UV-visible absorption spectrum of D. glomerata-derived CQDs is not common for carbon dots that usually exhibit two signals between 230 and 270 nm corresponding to π → π*transitions of aromatic C=C bonds and a second one between 300 and 330 nm corresponding to n → π* transitions of C=O bonds.[41] The broad absorption extending until ca. 650 nm likely originates from the partial conjugated π electrons in CQDs, from the doping or

the substitution of the carbon hexagonal structure by heteroatoms like N that allow to enhance the visible absorption [42] or from the increase in size of graphene sheets composing the CQDs.[43] The most intense PL emission is located at 478 nm and its intensity increases when increasing the excitation wavelength from 320 to 440 nm. The PL emission peak is not symmetric and a second contribution can be observed at ca. 562 nm (Figure 4b). The intensity of this second PL signal is the highest when exciting CQDs at ca. 520-540 nm. No excitation wavelength dependence on the PL emission wavelength is observed, contrary to what is classically observed in carbon-based photoluminescent materials. This behavior not only originates from particles of different sizes in the sample but also from the distribution of different emissive sites on each nanoparticle.[44] For D. glomerata-derived CQDs, when varying the PL excitation from 320 to 440 nm, the PL emission peak is located at 478 nm while the main PL emission is located at 562 nm when varying the excitation from 460 to 540 nm. After dialysis using a 1 kDa membrane, the contribution of the first signal is much greater in the retentate and only a weak PL emission could be observed after excitation of the dots at 520 nm (Figure 4c). Figure 4d shows that the PL located at 562 nm is mainly associated to small-sized CQDs with a molecular weight lower than 1 kDa present in the dialysate. These results suggest that both the size and the surface functionalization of sp^2 clusters contained in CQDs are uniform. The 3-D PL spectra of CQDs show that the optimal excitation and emission wavelengths are 430 nm and 470 nm, respectively (Fig. 4e-f) and further confirm that the PL emission wavelength does not depend on the excitation wavelength.

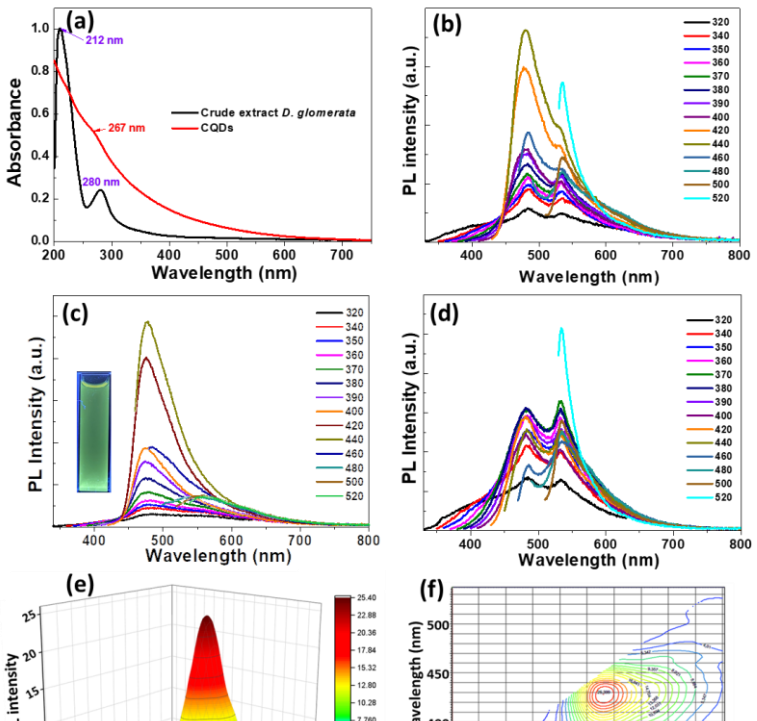

The homogeneous size and surface functionalization of sp^2 clusters was further confirmed by the PL lifetime measurements of CQDs which show a monoexponential decay characterized by the same decay time value (4.5 ns) for both emission wavelengths of 450 and 600 nm (Figure 5a-b). [45] The PL QY at room temperature of CQDs present in the retentate is of 18% using fluoresceine as reference. This relatively high PL QY value is likely linked to the N-doping of CQDs. The color of an aqueous solution of CQDs is light brown under room light while a bright green yellow fluorescence can be observed under UV light illumination (inset of Figure 4c).

As shown by transmission electron microscopy (TEM) (Figure 6a-b), CQDs exhibit a spherical/ellipsoidal morphology and are well dispersed. Their average diameter is 4.7 ± 1.2 nm as estimated from statistical distributions. The selected area electron diffraction (SAED) pattern shows only diffused rings, suggesting the amorphous character of CQDs (inset of Figure 6b). The HR-TEM image shows GQDs lattice fringe with a crystal plane spacing of 0.21 nm, value matching the (100) crystal plane of graphene (d100 = 0.213 nm). [46] The X-ray diffraction (XRD) pattern of CQDs shows a broad signal at ca. 21.5° which corresponds to the (111) plane of amorphous carbon,[47] which agrees well with the SAED pattern (Figure 6d). The broad hump at lower angles indicates the lack of long-range order as crystal characteristic, which confirms the amorphous nature of GQDs. The average hydrodynamic diameter of CQDs dispersed in water is of 5.6 nm, value slightly higher than that of dots in the dried state determined by TEM, due to the hydration corona surrounding CQDs (Figure 6e). Their Zeta potential is of -33 mV, value indicating a high density of carboxylate functions at the surface of CQDs which favors their stability in aqueous media.

Cyclic voltammograms (CV) in deoxygenated phosphate buffer 0.1 M (pH = 7.2) of the extract and of CQDs aqueous dispersions within the operational range -1.2 to +1.0 V are displayed in Figure 7. For the extract, in the oxidation part, the CV shows two pseudo- reversible redox processes at the formal potential of +0.24 (peak 1) and +0.53 V (peak 2) (Figure 7a) vs SCE, which was confirmed by differential pulse voltammetry (DPV) (Figure 7b).

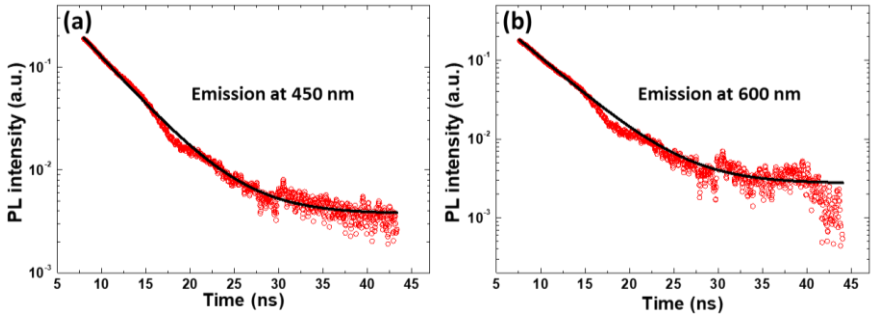

Figure 5. PL decays of CQDs measured at (a) 450 nm and (b) 600 nm.

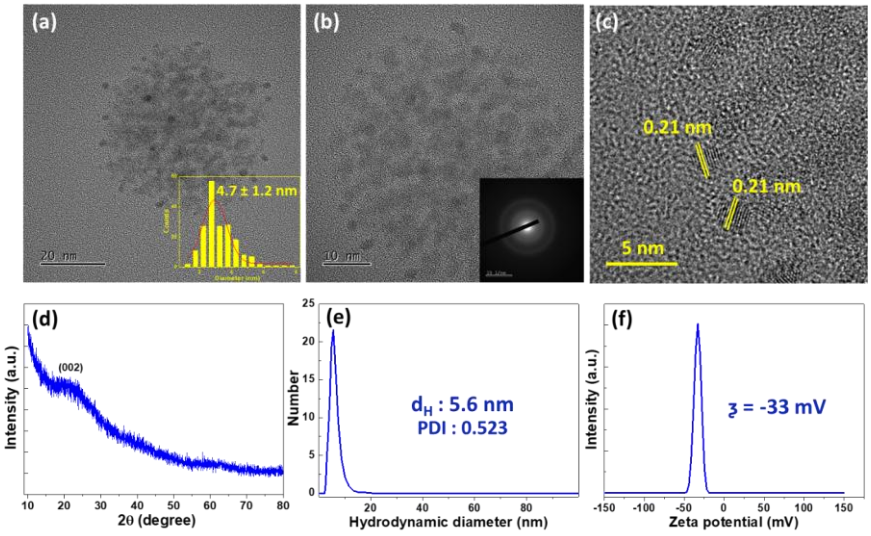

Figure 6. (a,b) TEM, (c) HR-TEM, (d) XRD pattern, (e) hydrodynamic diameter and (f) Zeta potential of CQDs. The insets of (a) and (b) are the size distribution and the SAED pattern, respectively.

Noteworthy is also that peak 2 is significantly broader than peak 1, indicating that electron transfer rates related to peak 2 are lower than that of peak 1. For CQDs, three redox processes, which display some reversibility can be observed at +0.21, +0.40 and +0.68 V vs SCE, indicating that the redox active functions of the extract and/or their environment were modified during the synthesis of CQDs (Figure 7c and Figure 7d for the corresponding DPV). These CV features are usually assigned to conjugated redox couples containing carboxylic acid or ketone functions and to CQDs peripheral units containing a quinone-like structure.[48,49] Non-conjugated carbonyl functions can be reversibly reduced but at significantly higher potential values (more than -2.0 V) while peroxides and epoxides are not reversibly reduced.[49]

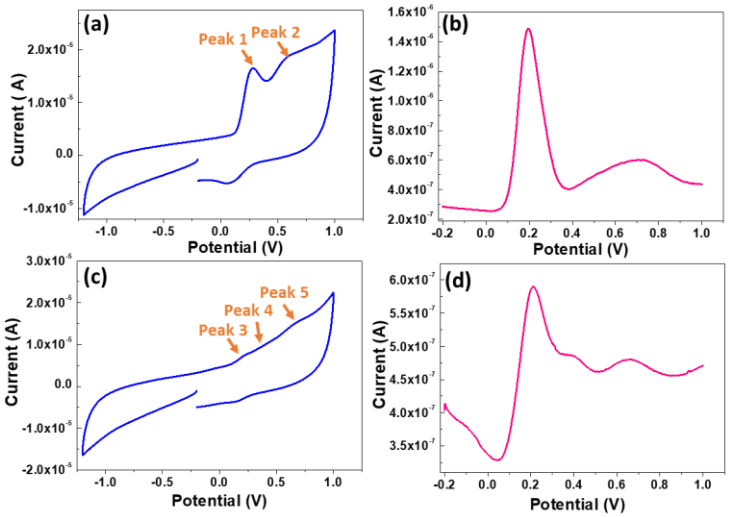

Figure 7. Cyclic voltammograms of aqueous dispersions of (a) *D. glomerata* extract and (b) CQDs within the operational range -1.2 to +1.0 V. (c) and (d) are the corresponding differential pulse voltammetry responses.

The influence of the pH of the aqueous solution on the PL emission was also investigated. As can be seen on Figure 8a, the PL emission markedly decreases at acidic pH (pH < 6) and at basic pH (pH > 11) but remains stable for pH values between 6 and 10. Figure S1 shows that the shape of the PL signal is not significantly affected by these pH changes. The decrease of the PL intensity observed at acidic pH

is likely linked to the protonation of carboxylate functions while the decrease observed at basic pH likely originates from the conversion of ammonium into amine groups. These results suggest that the electrostatic interactions between carboxylate and ammonium functions at pH values between 6 and 10 play a key role on the PL mechanism. Similar results were obtained in various buffers (PBS buffers with pH values varying from 5.5 to 8.0, borate buffer pH 9.1, carbonate buffer pH 10.2 and di/tripotassium buffer pH 12.7) (Figure S2a). The evolution of the PL emission spectra of CQDs in these buffer solutions was also monitored over time. As shown in Figures S2b and S2c, only PL spectra of CQDs stored in the di/tripotassium buffer are altered over time and a signal widening is observed. This second set of experiments also shows the high stability of CQDs in aqueous solutions of different pH over periods up to 90 days.

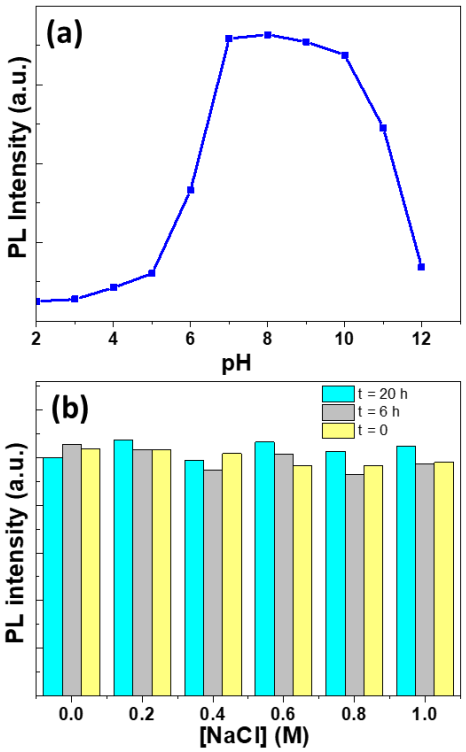

Figure 8. Influence of (a) the pH and (b) the ionic strength of the medium on the PL intensity of CQDs.

The impact of the ionic strength of the medium on the PL intensity was also investigated. For that purpose, CQDs were dispersed in NaCl aqueous solutions with

concentrations varying from 0 to 1 M. Figure 8b shows that the PL intensity is almost unchanged during the 20 h of storage, which further confirms the high colloidal stability of CQDs. Moreover, these results suggest that the electrostatic interactions between carboxylate and ammonium groups are not broken in media with a high ionic strength.

The free radical scavenging activity of CQDs was first evaluated using the 2,2-diphenyl-1-picrylhydrazyl (DPPH) method.[26,50] This assay is based on the color change of the DPPH radical into yellow upon reaction with a hydrogen donor. Ascorbic acid was used as reference antioxidant. Results obtained with concentrations of the extract, CQDs and ascorbic acid varying from 0 to 0.5 mg/mL are depicted in Figure 9a. As can be observed, the radical scavenging activity of the three compounds was found to increase in a dose-dependent manner. At concentrations below 0.4 mg/mL, the fastest disappearance of DPPH is observed with the *D. glomerata* extract which exhibits a higher antioxidant activity than ascorbic at low concentrations. The lower activity observed with CQDs shows that many hydrogen donor groups (OH, NH_2) of the extract were transformed during its conversion into CQDs. For concentrations of ascorbic acid, *D. glomerata* extract and CQDs of 0.5 mg/mL, the scavenging activities were found to be of 83, 75 and 25%, respectively. The amounts of ascorbic acid or of the *D. glomerata* extract required to decrease the concentration of DPPH by 50% (EC50) were estimated to be 0.16 and 0.29 mg/L, respectively.

The photocatalytic degradation of the Orange II dye was used as reference reaction to further evaluate the antioxidant activity of the extract and of CQDs (Figure 9b).[51] Under simulated solar light irradiation, ca. 89% of the Orange II dye is decomposed by graphitic carbon nitride (g-C3N4) after 70 min irradiation, indicating that reactive oxygen species (ROS) produced by irradiation of g-C_3N_4 ($O_2^{\bullet-}$ radicals, singlet oxygen 1O2 and holes in the valence band of the semiconductor) oxidize the dye.

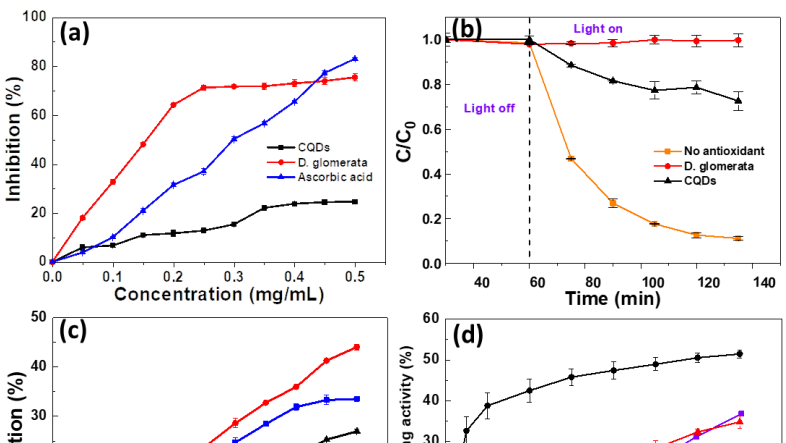

When the photodegradation was conducted in the presence of the extract, no decomposition of the dye was observed. The antioxidative properties of CQDs is slightly weaker and ca. 27% of the dye is decomposed after 70 min irradiation. This decrease of the photocatalytic activity likely originates from the transformation of the oxidative species generated under light illumination ($O_2^{\bullet -}$ radicals, $^1O_2$, holes) into species with a lower oxidizing power or without any oxidizing power (^-OH, $^3O_2$, O_2^{2-} and then HO_2^- and H_2O_2).

The antioxidant activity of the extract and of CQDs was further evaluated using the $KMnO_4$ reductive assay.[52] The reduction of $KMnO_4$ that leads to a color change from purple to colorless was monitored by UV-visible absorption at 515 nm. The spectral changes observed confirm that Mn(+7) is reduced into Mn(+2) by the extract and CQDs (Figure 9c). Results show that both the extract and CQDs exhibit high antioxidant activity. Noteworthy is that the antioxidant activity of the extract is higher than that of ascorbic acid. It should also be noted that the antioxidant activity of CQDs is marked in reactions in which its ability as an electron donor is involved (reduction of $KMnO_4$, reduction of ROS). Its ability to give hydrogen atoms to neutralize the free DPPH radical is significantly weaker.

In a final series of experiments, we evaluated the ability of CQDs to chelate Cu^{2+} ions. In their unbound form, Cu^{2+} ions may be reduced in vivo into Cu^+ ions and react with hydrogen peroxide H_2O_2 to produce hydroxyl radicals via the Fenton reaction (equation 1), which conducts to oxidative stress.

$$Cu^+ + H_2O_2 + H^+ \longrightarrow Cu^{2+} + {}^{\bullet}OH + H_2O \qquad (1)$$

Cu^{2+} ions may also bind to enzymes leading to their inactivation. Several pathologies including Parkinson's and Alzheimer diseases are linked to an overload of Cu^{2+}

ions.[53] In this context, the development of Cu^{2+}-chelating nanoparticles as therapeutic agents able to decrease the oxidative damages caused by unbound Cu^{2+} ions has recently gained interest.[54] The ability of CQDs and of the extract to chelate Cu2+ ions was evaluated using the Cu^{2+}-murexide complex that dissociates in the presence of a Cu^{2+} chelator.[55] Carnosine, well known to produce stable complexes with Cu^{2+} ions, was used as reference.[56] As can be seen from Figure 9d, the Cu^{2+} chelating activity of CQDs is higher than that of the extract or of carnosine, especially at low concentrations. For CQDs, a fast increase of the chelating activity is observed up to a concentration of CQDs of 0.12 mg/mL (chelating activity of 32.6%). Thereafter, the increase is slower and reaches a quasi-plateau (chelating activity of 51% for a concentration in CQDs of 1.75 mg/mL). The Cu^{2+} chelating activities of the extract and of carnosine are close, increase almost linearly and reach a value of ca. 35% for a concentration of 1.75 mg/mL. The strong affinity of CQDs for Cu^{2+} cations is likely linked to the high density of carboxylate functions at the surface of CQDs combined with the presence of N atoms in the graphitic framework that allow to form stable complexes with Cu^{2+} ions.[57]

Results described in Figure 9 indicate that the density of OH and NH_2 functions at the periphery of CQDs sheets is weak as CQDs exhibit a modest scavenging activity towards the DPPH radical (Figure 10). Their reducing activity through electron transfer from the graphitic framework is higher as demonstrated by their ability to reduce $KMnO_4$ and $O_2^{\bullet-}$ radicals. The addition of $O_2^{\bullet-}$ radicals at sp^2 sites of the graphitic network followed by the decomposition of the peroxy intermediates could also be involved in the reduction. The high density in carboxylate groups and the N doping of the sp^2 framework allow CQDs to strongly coordinate with Cu^{2+} ions.

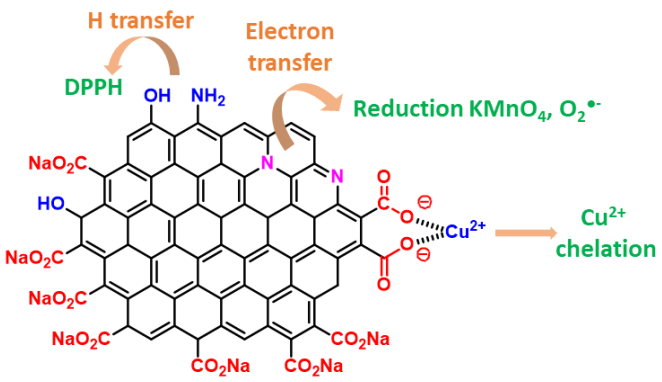

Figure 10. Mechanisms involved in the antioxidant and chelating activities of *D. glomerata* derived CQDs.

Conclusion

In conclusion, negatively-charged CQDs were efficiently prepared by a hydrothermal method using the D. glomerata extract as precursor. CQDs exhibit an average size of ca. 4.7 nm as well as different optical properties compared to biomass-derived carbon dots described in the literature. CQDs show two PL emissions at 478 and 562 nm and their relative intensity depends on the excitation wavelength. These results indicate that the surface functionalization of sp2 clusters in CQDs is uniform, which was confirmed by the monoexponential decay of their PL lifetime. The prepared CQDs can effectively reduce free radicals like $O_2^{\bullet-}$ or oxidants like $KMnO_4$. Moreover, CQDs show higher Cu^{2+} chelating activity than the starting extract or carnosine, which is attributed to the abundant carboxylate functions on their surface. The D. glomerata-derived CQDs may serve as antioxidant and Cu^{2+}-chelating agents in various therapeutic applications.

Experimental Section

Reagents

Potassium permanganate ($KMnO_4$, 99.5%, Merck), ascorbic acid (99+%, Fisher Scientific), hydrogen peroxide (H_2O_2 30%, VWR), L-carnosine (99%, Merck), murexide (Fisher Scientific), copper sulphate ($CuSO_4$ 99%, Merck), sodium hydroxide (NaOH 98.5%, VWR), 2,2-diphenyl-1-picrylhydrazyl (DPPH 95%, Fisher Scientific), sodium acetate (99%, Thermo Scientific), acetic acid (99.8%, Merck), absolute ethanol (99.98%, VWR), potassium chloride (99%, Fisher Scientific), Orange II (95%, Merck), and hydrochloric acid (37%, Merck) were used without further purification. Aqueous solutions were prepared using ultrapure water (18 MΩ cm, 20°C). Graphitic carbon nitride was prepared as previously described [49].

Preparation of the *D. glomerata* extract

The dried pods of D. glomerata were purchased from a spice vendor in Cameroon. The pods were dried at 40°C for 12 h, pounded using a wooden mortar and sieved

using a 400 µm mesh. The refuse was pounded till almost use up. The fraction with a size below 400 µm was mixed with 1 L of methanol, stirred for 12 h using a magnetic stirrer, and filtered using Whatman paper N°4. The solid remaining on the filter was again dispersed in 1 L of methanol and stirred for another 12 h, then filtered. The two methanol fractions were mixed and evaporated under vacuum at 40°C to obtain the crude methanol extract of D. glomerata that was stored in a glass container.

Preparation of CQDs

About 400 mg of the crude methanol extract of D. glomerata were mixed with 40 mL of 4 M NaOH solution before being transferred into a 100 mL Teflon-sealed autoclave and heated at 200°C for 7 h to obtain crude CQDs. The crude CQDs were dialysed against ultrapure water for 65 h using a 1000 Da dialysis membrane. The dialysis water was changed after every 2 h during the first 6 h of dialysis and thereafter every 10 h. At the end of the dialysis, the retentate was evaporated with a rotary evaporator at 40℃to obtain the purified CQDs.

Characterizations

The morphology and the microstructure of CQDs were studied by TEM (JEOL-ARM200 Cold FEG microscope operating at 200 keV, equipped with double spherical aberration correctors and fitted with a JEOL SDD CENTURIO EDS system and a Gatan GIF Quantum). XRD patterns were recorded on a Panalytical X'Pert Pro MPD diffractometer using a Cu Kα radiation (λ = 0.15418 nm) source operating at 30 kV and 10 mA. XPS measurements were carried out with a Gammadata Scienta SES 200-2 spectrometer.

TGA was conducted under air from 20 to 1000°C at a heating rate of 10°C/min using a TGA/DSC1 STAR equipment (Mettler-Toledo). Zetasizer Nano-ZS (Malvern Panalytical, United Kingdom), equipped with a He/Ne ion laser at λ = 532 nm in a backscattering configuration with a measurement angle of 173°, was utilized to investigate the size and the Zeta potential of CQDS. The experiments were conducted at 25°C after a 120-second equilibration period. The measurements were conducted in triplicate using a disposable folded capillary cell (DTS1070, Malvern Panalytical) and presented as mean expressed in % Number ± standard deviation

All the optical measurements were performed at room temperature and under ambient conditions. UV-visible absorption spectra were recorded on a Thermo Scientific Evolution 220 spectrophotometer. PL emission spectra were measured on a Shimadzu RF-6000 and on a SAFAS flx Xenius equipments. PL spectra were spectrally corrected and relative PL QYs were determined using fluorescein in ethanol (PL QY = 79%) as reference. For the time-resolved PL experiments, CQDs were pumped by the 355 nm line of a frequency-tripled YAG (yttrium aluminium garnet): Nd laser. The laser pulse frequency, energy and duration were typically equal to 10 Hz, 50 μJ and 10 ns, respectively. The PL signal was analysed by a monochromator equipped with a 600 grooves/mm grating and by a photomultiplier tube cooled at 190 K. The rise time of the detector is equal to around 3 ns.

The redox properties of the extract and CQDs were investigated with an Autolab PGSTAT 100 workstation (Metrohm) controlled by an external PC and using a standard three-electrode setup at 25°C. Working vitreous carbon electrode (3 mm diameter) was polished with 6 μm diamond paste. A Pt wired served as counter electrode while a calomel electrode (SCE) was employed as reference electrode and separated from the bulk by a double bridge. Phosphate buffer solution (pH = 7.2) was employed as the supporting electrolyte at a concentration of 10-1 mol/L. Typically, solutions were purged with argon flow 10 min, and the voltammogram was recorded at ambient temperature with a scan rate of 20 mV/s.

Free radical scavenging activity

2,2-Diphenyl-1-picrylhydrazyl (DPPH) radical scavenging

The free radical scavenging activity of the D. glomerata extract and of CQDs was evaluated using the DPPH assay with slight modifications. [26,50] A 0.5 mM solution of DPPH in ethanol was used for the tests. Briefly, 0.1 mL of each sample in acetate buffer concentration (0.05 mM, pH 5.5) was mixed with 1.9 mL of absolute ethanol and 1 mL of the DPPH solution. The mixture was vortexed after adding DPPH and kept in dark at 25°C for 30 min before measuring the absorbance at 517 nm. A blank test was conducted using ultrapure water. All measurements were replicated three times. The DPPH scavenging activity (%) was determined using equation (2).

$$Cu^{2+}\text{chelating activity }(\%) = \left[\frac{\left(\frac{Ac485}{Ac520} - \frac{As485}{As520}\right)}{\left(\frac{Ac485}{Ac520}\right)} x\ 100\right] (2)$$

where Abs control and Abs sample are the absorbances of the sample and of the control at 517 nm, respectively.

Scavenging of superoxide radicals and singlet oxygen

Graphitic carbon nitride (g-C_3N_4), a common used semiconductor photocatalyst, was used in this work.[51] Under simulated solar light illumination, electrons promoted in the conduction of g-C_3N_4 react with adsorbed O_2 to produce superoxide ($O_2^{\bullet-}$) radicals. Superoxide radicals can be reduced by holes in the valence band and produce singlet oxygen ($^1O_2$). Superoxide radicals and singlet oxygen are able to decompose organic dyes due to their high oxidant properties (E^0 = -0.33 vs. NHE for $O_2^{\bullet-}/O_2$ and E0 = +1.88 V vs NHE for $^1O_2/O_2$).

The $O_2^{\bullet-}$ radicals and $^1O_2$ scavenging ability of CDs and of the extract were evaluated in the g-C_3N_4-mediated photocatalytic degradation of the Orange II dye under simulated solar light irradiation. In a typical experiment, 20 mg of g-C_3N_4 were dispersed in 40 mL of the Orange II dye (concentration of 10 mg/L) under sonication. Next, 5 mg of CQDs or of the extract were introduced and the mixture stirred for 1 h in the dark to achieve the adsorption-desorption equilibrium. After that period, the mixture was exposed to simulated solar light irradiation (light irradiance of 15 mW/cm^2 at 365 nm). Each 15 min, aliquots (2 mL) were removed, centrifuged (15,000 rpm) and the photocatalytic degradation of Orange II was monitored by UV-visible spectroscopy.

Potassium permanganate reducing ability

The antioxidant activity of CQDs and of the extract was also assessed with the $KMnO_4$ reduction assay following the protocol described in ref. 50 with some modifications. Ascorbic acid was used as reference. Briefly, 2 mL of a 5 mM $KMnO_4$ solution were mixed with 400 µL of aqueous solutions of CQDs, of the extract or of ascorbic acid (used at concentrations varying from 0 to 0.25 mg/mL). The mixture was vortexed for 5 s before being incubated at 37°C for 30 min. After centrifugation at 5000 rpm for 3 min, the supernatant was analyzed by UV-visible absorption

spectroscopy at 515 nm. Upon reduction, $KMnO_4$ solutions change from purple to colorless. All measurements were replicated three times. The reducing activity was calculated using equation (3):

$$Cu^{2+}\text{chelating activity }(\%) = \left[\frac{\left(\frac{Ac485}{Ac520} - \frac{As485}{As520}\right)}{\left(\frac{Ac485}{Ac520}\right)} x\ 100\right] \quad (3)$$

Cu^{2+} chelating activity

The Cu^{2+} chelating activity of CQDs, of the D. glomerata extract and of carnosine was determined according to ref. 53. The assay is based on the dissociation of the Cu^{2+}-murexide complex in the presence of a Cu chelator and the appearance of free murexide in solution. UV-visible absorptions at 485 nm and 520 nm were used to monitor the Cu^{2+}-murexide complex and free murexide, respectively. The ratio of the absorbance Abs(485)/Abs(520) is proportional to the concentration of free Cu^{2+} in the solution. Aqueous solutions of CQDs, of the D. glomerata extract and of carnosine used as reference were prepared at concentrations varying from 0 to 0.1 mg/mL. A volume of 143 µL of sample solution was pipped into a test tube. Then, 143 µL of 3 mM $CuSO_4$ solution in hexamine buffer (10 mM hexamine, 10 mM KCl, pH 5) were added followed by 14 µL of a 1 mM aqueous solution of murexide. After incubation for 3 min at room temperature, UV-visible absorption spectra were recorded against the hexamine buffer solution and ultra-pure water used as blank. The Cu^{2+} chelating activity was determined using equation (4).

$$Cu^{2+}\text{chelating activity }(\%) = \left[\frac{\left(\frac{Ac485}{Ac520} - \frac{As485}{As520}\right)}{\left(\frac{Ac485}{Ac520}\right)} x\ 100\right] \quad (4)$$

where Ac is the absorbance of the control tube with not sample and As is the absorbance of the tube containing the sample (CQDs, D. glomerata extract or carnosine).

Funding

No funding was received for conducting the study.

Authors contribution

Corresponding author supervised the complete data. Material preparation, data collection and analysis were performed by S; Djiazet, C. Desmarets, H. Rinnert, J.

Jasniewski, G. Medjahdi, and L. Balan. The first draft of the manuscript was written by S. Djiazet and all authors commented on previous versions of the manuscript. All other authors have contributed and approved the final manuscript.

Supporting Information

Figure S1. Influence of pH on the PL intensity of CQDs. Figure S2. Influence of the pH of various buffers and over time on the PL intensity of CQDs.

Acknowledgements

Steve Djiazet wishes to acknowledge the program MOGPA for financial support. The authors thank Camille Rubio (LRGP, Université de Lorraine) for CHONS analyzes. This project has benefited from the expertise and the facilities of the Platform MACLE-CVL which was co-funded by the European Union and Centre-Val de Loire Region (FEDER)

Conflict of Interests

The authors declare no competing financial interest or personal relationships that could have appeared to influence the work reported in the paper.

Data Availability Statement

All data analysed during the study are included in the main paper and in the Supporting Information file. All datasets are available from the corresponding author on reasonable request.

Keywords: carbon quantum dots • D. glomerata • photoluminescence • antioxidant • Cu^{2+} chelation

References

[1] D. Kuatea, B.C.O. Etoundia, Y.B. Soukontouab, J.L. Ngondia, J.E. Oben, CYTA - J. Food 2010, 8, 23–37.

[2] S.C. Kothari, P. Shivarudraiah, S.B. Venkataramaiah, S. Gavara, S.N. Arumugam, M.G. Soni, Food Chem. Toxicol. 2014, 69, 120-131.

[3] M. Deli, E. Djantou Baudelaire, R.M. Nguimbou, N. Njintang Yanou, J. Scher, Food Sci. Nutr. 2020, 8, 3287-3297.

[4] S. Karakaya, Crit. Rev. Food Sci. Nutr. 2004, 44, 453-464.

[5] F. Shahidi, H. Peng, J. Food Bioact. 2018, 4, 11-68.

[6] Y. Zhang, L. Chen, R. Sun, R. Lv, T. Du, Y. Li, X. Zhang, R. Sheng, Y. Qi, ACS Biomater. Sci. Eng. 2022, 8, 638-648.

[7] Z. Bedlovicová, I. Strapác, M. Baláž, A Salayová, Molecules 2020, 25, 3191.

[8] C. Gunawan, M.S. Lord, E. Lovell, R.J. Wong, M.S. Jung, D. Oscar, R. Mann, R. Amal, ACS Omega 2019, 4, 9473-9479.

[9] S.Y. Lim, W. Shen, Z. Gao, Chem. Soc. Rev. 2015, 44, 362-381.

[10] L. Wang, W. Li, L. Yin, Y. Liu, H. Guo, J. Lai, Y. Han, G. Li, M. Li, J. Zhang, R. Vajtai, P.M. Ajayan, M. Wu, Sci. Adv. 2020, 6, eabb6772.

[11] M.J. Molaei, Anal. Methods 2020, 12, 1266-1287.

[12] L.J. Desmond, A.N. Phan, P. Gentile, Environ. Sci.: Nano 2021, 8, 848-862.

[13] X. Kou, S. Jiang, S.-J. Park, L.-Y. Meng, Dalton Trans. 2020, 49, 6915-6938.

[14] X. Li, M. Rui, J. Song, Z. Shen, H. Zeng, Adv. Funct. Mater. 2015, 25, 4929-4947.

[15] T. Yuan, T. Meng, P. He, Y. Shi, Y. Li, X. Li, L. Fan, S. Yang, J. Mater. Chem. C 2019, 7, 6820-6835.

[16] T. Ghosh, T. Kanti Das, P. Das, P. Banerji, N.C. Das, Carbon Lett. 2022, 32, 953.

[17] Z. Liu, W. Hou, H. Guo, Z. Wang, L. Wang, M. Wu, ACS Appl. Mater. Interfaces 2023, 15, 33868.

[18] M. Ehtisham Khan, A Mohammad, T. Yoon, Chemosphere 2022, 302, 134815.

[19] M. Li, T. Chen, J.J. Gooding, J. Liu, ACS Sens. 2019, 4, 1732-1748.

[20] S. Amren Shaik, S. Sengupta, R.S. Varma, M.B. Gawande, A. Goswami, ACS Sustainable Chem. Eng. 2021, 9, 3-49.

[21] R. Atchudan, T.N. Jebakumar Immanuel Edison, M. Shanmugam, S. Perumal, T. Somanathan, Y. Rok Lee, Physica E 2021, 126, 114417.

[22] N. Sohal, S. Singla, S.J. Malode, S. Basu, B. Maity, N.P. Shetti, ACS Appl. Nano Mater. 2023, 6, 10925-10943.

[23] A. Sachdeva, P. Gopinath, Analyst 2015, 140, 4260–4269.

[24] L.A. Avinash Chunduri, A. Kurdekar, S. Patnaik, B. Vishnu Dev, T. Mimani Rattan, V. Kamisetti, Mater. Focus 2016, 5, 55–61.

[25] T. Arumughama, M. Alagumuthu, R.G. Amimodu, S. Munusamy, S. Kulathu Iyer. Sustainable Mater. Technol. 2020, 23, e00138.

[26] Z.M. Marković, M. Labudová, M. Danko, D. Matijašević, M. Mičušík, V. Nádaždy, M. Kováčová, A. Kleinová, Z. Špitalský, V. Pavlović, D.D. Milivojević, M. Medić, B.M. Todorović Marković, ACS Sustainable Chem. Eng. 2020, 8, 16327–16338.

[27] C. Murru, R. Badía-Laíño, M.E. Díaz-García, Antioxidants 2020, 9, 1147.

[28] N. Sharma, G. Sankar Das, K. Yun, Appl. Microbiol. Biotechnol. 2020, 104, 7187–7200.

[29] P. Surendran, A. Lakshmanan, S. Sakthy Priya, P. Geetha, P. Rameshkumar, K. Kannan, T. Ashok Hegde, G. Vinitha, Inorg. Chem. Commun. 2021, 124, 108397.

[30] M.H. Son, S.W. Park, Y.K. Jung, Nanotechnology 2021, 32, 415102.

[31] S. Rajamanikandan, M. Biruntha, G. Ramalingam, J. Clust. Sci. 2022, 33, 1045–1053.

[32] X. Li, X. Liu, Y. Su, T. Jiang, D. Li, X. Ma, Ind. Crops Prod. 2022, 188, 115568.

[33] M. Moniruzzaman, S. Deb Dutta, J. Hexiu, K. Ganguly, K.-T. Lim, J. Kim, Biomater. Sci. 2022, 10, 3527-3539.

[34] F. Wen, P. Li, Y. Zhang, H. Zhong, H. Yan, Wei Su. J. Mol. Struct. 2023, 1273, 134247.

[35] A. Khoshkalampour, M. Ghorbani, Z. Ghasempour, Food Chem. 2023, 404, 134742.

[36] Q. Li, X. Shen, D. Xing, Dyes Pigm. 2022, 208, 110784.

[37] S.L. Hu, A. Trinchi, P. Atkin, I. Cole, Adv. Mater. 2015, 54, 2970-2974.

[38] X. Qu, C. Gao, L. Fu, Y. Chu, J.-H. Wang, H. Qiu, J. Chen, ACS Appl. Mater. Interfaces 2023, 15, 18608-18619.

[39] S. Liu, J. Tian, L. Wang, Y. Luo, J. Zhai, X. Sun, J. Mater. Chem. 2011, 21, 11726-11729.

[40] M. Ihsan, A. Niaz, A. Rahim, M. Iqbal Zamen, M. Balal Arain, Sirajuddin, T. Sharif, M. Najeeb, RSC Adv. 2015, 5, 91158-91165.

[41] J.M. Arroyave, R.E. Ambrusi, Y. Robein, M.E. Pronsato, G. Brizuela, M.S. Di Nazio, M.E. Centurion, Appl. Surf. Sci. 2021, 564, 150195.

[42] S. Ozonder, C. Unlü, C. Güleryüz, L. Trabson, ACS Omega 2023, 8, 2112-2118.

[43] R. Zhang, S. Qi, J. Jia, B. Torre, H. Zeng, H. Wu, X. Xu, J. Alloys Compd. 2015, 623, 186-191.

[44] L. Li, G. Wu, G. Yang, J. Peng, J. Zhao, J.-J. Zhu, Nanoscale 2013, 5, 4015-4039.

[45] D. Qu, M. Zheng, P. Du, Y. Zhou, L. Zhang, D. Li, H. Tan, Z. Zhao, Z. Xied, Z. Sun, Nanoscale 2013, 5, 12272–12277.

[46] A.-M. Alam, B.-Y. Park, Z.K. Ghouri, M. Park, H.-Y. Kim, Green Chem. 2015, 17, 3791.

[47] A. Sachdev, I. Matai, S.U. Kumar, B. Bhushan, P. Dubey, G. Gopinath, RSC Adv. 2013, 3, 16958-16961.

[48] A.-Y.-S. Eng, A. Ambrosi, C.-K. Chua, F. Šaněk, Z. Sofer, M. Pumera, Chem. Eur. J. 2013, 19, 12673-12683.

[49] Y. Tian, L. Li, X. Guo, A. Wójtowicz, L. Estevez, M.J. Krysmannd, A. Kelarakis, Chem. Commun. 2018, 54, 9067-9070.

[50] K. Pyrzynska and A. Pekal, Anal. Methods 2013, 5, 4288–4295.

[51] H. Moussa, B. Chouchene, T. Gries, L. Balan, K. Mozet, G. Medjahdi, R. Schneider, ChemCatChem 2018, 10, 4987-4997.

[52] B. Das, P. Dadhich, P. Pal, P. Kumar Srivas, K. Bankoti, S. Dhara, J. Mater. Chem. B 2014, 2, 6839-6847.

[53] M.E. Letelier, S. Sánchez-Jofré, L. Peredo-Silva, J. Cortés-Troncoso, P. Aracena-Parks, Chem.-Biol. Interact. 2010, 188, 220-227.

[54] Y.J. Chung, B.I. Lee, C.B. Park, Nanoscale 2019, 11, 6297-6306.

[55] R. El-Hnayn, L. Canabady-Rochelle, C. Desmarets, L. Balan, H. Rinnert, O. Joubert, G. Medjahdi, H. Ben Ouada, R. Schneider. Nanomaterials 2020, 10, 104.

[56] C. Abate, D. Aiello, M. Cordaro, O. Giuffrè, A. Napoli, C. Foti, J. Mol. Liq. 2022, 368, 120772.

[57] R.C. Holz, J.M. Brink, F.T. Gobena, C.J. O'Connor, Inorg. Chem. 1994, 33, 6086-6092.